Nucleic Acids Research, 2006, Vol. 34, No. 1 ***275–285***
doi:10.1093/nar/gkj436

The role of positively charged amino acids and electrostatic interactions in the complex of U1A protein and U1 hairpin II RNA

Michael J. Law[1,2], Michael E. Linde[1,2], Eric J. Chambers[3], Chris Oubridge[4], Phinikoula S. Katsamba[1,2], Lennart Nilsson[5], Ian S. Haworth[1,3] and Ite A. Laird-Offringa[1,2,*]

[1]Department of Biochemistry and Molecular Biology and [2]Department of Surgery, Keck School of Medicine and [3]Department of Pharmaceutical Sciences, School of Pharmacy, University of Southern California, Los Angeles, CA 90089-9176, USA [4]MRC Laboratory of Molecular Biology, Hills Road, Cambridge CB2 2QH, UK and [5]Karolinska Institutet, Department of Biosciences at Novum, SE-141 57 Huddinge, Sweden

Received October 14, 2005; Revised and Accepted December 22, 2005

ABSTRACT

Previous kinetic investigations of the N-terminal RNA recognition motif (RRM) domain of spliceosomal protein U1A, interacting with its RNA target U1 hairpin II, provided experimental evidence for a 'lure and lock' model of binding in which electrostatic interactions first guide the RNA to the protein, and close range interactions then lock the two molecules together. To further investigate the 'lure' step, here we examined the electrostatic roles of two sets of positively charged amino acids in U1A that do not make hydrogen bonds to the RNA: Lys20, Lys22 and Lys23 close to the RNA-binding site, and Arg7, Lys60 and Arg70, located on 'top' of the RRM domain, away from the RNA. Surface plasmon resonance-based kinetic studies, supplemented with salt dependence experiments and molecular dynamics simulation, indicate that Lys20 predominantly plays a role in association, while nearby residues Lys22 and Lys23 appear to be at least as important for complex stability. In contrast, kinetic analyses of residues away from the RNA indicate that they have a minimal effect on association and stability. Thus, well-positioned positively charged residues can be important for both initial complex formation and complex maintenance, illustrating the multiple roles of electrostatic interactions in protein–RNA complexes.

INTRODUCTION

RNA-binding proteins (RNA-BPs) are critical to many regulatory processes in the cell, including transcriptional termination, mRNA splicing, mRNA export from the nucleus into the cytoplasm, intracellular localization of transcripts, mRNA translation, mRNA stability, and processing of tRNA and rRNA (1). RNA-BPs also play key roles in maintaining the structure and activity of important intracellular machinery, including the spliceosome, ribosome, telomerase and the signal recognition particle (1–5). In order to perform their variety of functions, RNA-BPs must bind to their specific RNA targets with affinities that correspond to the function of the complex, ranging from relatively nonspecific, transient binding (such as the binding involved in general RNA processing) to highly specific and stable interactions (such as those involved in the formation of intracellular machinery). Owing to the strong negative electrostatic field associated with the RNA phosphate backbone (6,7), charged interactions are likely to be important for proper protein binding and ultimately for complex function. Indeed, electrostatic interactions have been shown to play a role in the function of RNA-BPs involved in intracellular processes such as translational initiation and elongation, ribosomal assembly and tRNA synthetase complex formation (8–12). As these electrostatic forces can extend

*To whom correspondence should be addressed. Tel: +1 323 865 0655; Fax: +1 323 865 0158; Email: ilaird@usc.edu
Present addresses:
Michael E. Linde, Graduate Program in Immunology, Johns Hopkins School of Medicine, Richard Starr Ross Research Building, Suite 1071S, Baltimore, MD 21205, USA
Phinikoula S. Katsamba, Center for Biomolecular Interaction Analysis, School of Medicine, University of Utah, Salt Lake City, UT 84132, USA

up to 11 Å from the RNA phosphate backbone (13), they are thought to play a role in the initial attraction between RNA and positively charged residues on RNA-BPs. Previous kinetic studies from our laboratory have demonstrated that electrostatic interactions play a role in bringing the spliceosomal U1A protein and its RNA target in the U1 small nuclear RNA (U1 snRNA) together (14).

U1A, the A protein of the U1 small nuclear ribonucleoprotein (U1 snRNP) complex, is one of the most-studied representatives of the largest family of RNA-BPs, characterized by the presence of one or more RNA recognition motifs (RRMs). RRMs are the most commonly found RNA-binding domain in eukaryotes and are present in hundreds of proteins that perform a wide variety of functions in the cell (2,15,16). U1A consists of two RRMs separated by a central hinge region, and studies of fragments of the U1A protein have suggested that the N-terminal RRM of U1A is necessary and sufficient for specific binding to its target in U1snRNA: U1 hairpin II (U1hpII) (17–19). Here we focus on the interaction of the N-terminal RRM (herein referred to as U1A) and U1hpII. The well-characterized U1A/U1hpII complex provides an ideal model to investigate the role of electrostatic interactions in protein–RNA binding (2,20–23). Examination of the U1A/U1hpII crystal and NMR structures reveals that a number of positively charged residues are located in close proximity to the RNA-binding site and that these positive charges are conserved in metazoans (5,22,24,25). Equilibrium and computational studies probing the overall electrostatic contribution of these residues in the U1A model system have indicated that electrostatic forces contribute importantly to the energy needed for the interaction (14,20,21,26). A steep salt dependence of U1A/U1hpII binding confirms this notion (14,21). Indeed, substitution of positively charged U1A residues with uncharged amino acids generally results in decreased affinity of U1A for U1hpII (14,26–28). Molecular dynamics simulations of the U1A/U1hpII interaction have indicated that electrostatic interactions may allow favorable positioning of residues involved in specific close range interactions (20). The results of these studies have emphasized the importance of charged residues in U1A/RNA binding. However, much remains to be elucidated about the mechanism by which electrostatic interactions contribute to the formation and/or stabilization of protein–RNA complexes. Surface plasmon resonance-based biosensor (Biacore) analysis has been a powerful tool to examine the kinetics of the U1A/U1hpII interaction. Using this method we have provided experimental support for a 'lure and lock' model, in which electrostatic interactions mediate early interactions, while close range interactions lead to locking down of the RNA target (14,29). We have recently suggested a model for the stepwise process of U1A/U1hpII locking (30). In an effort to further dissect the lure step of this interaction, here we investigate the role of electrostatic interactions in the U1A/U1hpII complex. To focus on purely electrostatic components of the interaction, we concentrated on positively charged amino acids that do not make hydrogen bonds to the RNA in the protein–RNA complex. Our kinetic analyses of mutant proteins interacting with U1hpII and salt dependence experiments indicate that, depending on their location, such residues function not only in luring the RNA to the protein, but they also help stabilize the U1A/U1hpII complex. This finding provides new evidence for multiple roles of electrostatic interactions in protein–RNA complexes.

MATERIALS AND METHODS

Construction of U1A mutants and protein purification

Throughout these studies, an N-terminal fragment of the human U1A protein containing the first RRM was used (14). This fragment has been demonstrated to be necessary and sufficient for specific and high-affinity binding to U1hpII (18,19). The protein was either obtained as an untagged amino acid 2–98 fragment (single point mutant proteins) (22) or as a C-terminally tagged protein (amino acids 1–101) produced as described previously (14). The tagged 101 fragment contained engineered BstEII and BssHII restriction sites that result in two conservative amino acid substitutions: Phe75Tyr and Lys88Arg, respectively. No kinetic differences were observed when comparing tagged and untagged versions of the protein (data not shown). All mutants were generated by site-directed mutagenesis and confirmed by sequencing. The concentration of each protein was estimated using the Bradford assay (BioRad, Hercules, CA) and confirmed by Coomassie blue staining of an extensive protein dilution series next to a standard on SDS–PAGE gels.

Biosensor analysis

Binding experiments were performed on a BIACORE 2000 instrument (Biacore Inc., Piscataway, NJ). U1hpII RNA was chemically synthesized carrying a 5′-biotin tag (Dharmacon Research, Boulder, CO) to allow immobilization of the RNA onto streptavidin-coated sensor chips (SA chips, Biacore Inc.). RNA was diluted to a final concentration of 1 μM in HBS buffer [10 mM HEPES, pH 7.4, 150 mM NaCl, 3 mM EDTA and 0.005 % surfactant P20 (Biacore, Inc.)] followed by heating at 80°C for 10 min and cooling to room temperature to allow annealing of the stem. The sample was then diluted 500-fold in running buffer [10 mM Tris–HCl, pH 8.0, 150 mM NaCl, 5% glycerol, 125 μg ml^{-1} yeast tRNA (Roche, IN), 62.5 μg ml^{-1} acetylated BSA (New England Biolabs, MA), 1 mM DTT, 0.05% (v/v) surfactant P20] and injected over the sensor chip surface at 10 μl min^{-1} at 20°C. To provide an optimal comparison of the results obtained from all different U1A mutants, we prepared two surface densities on the sensor chip, an intermediate density RNA surface (100–125 resonance units) that would yield sufficient signal, even when proteins with lower affinities were used, and a low density RNA surface (35–50 resonance units). To test for the specificity of the RNA-binding interaction, binding of all proteins to a control surface consisting of a U1hpII RNA in which the order of the loop nucleotides had been reversed from 5′-AUUGCACUCC-3′ to 5′-CCUCACGUUA-3′ ('reverseU1 hpII') was also assessed. Reversion of the loop sequence changes 8 of the 10 loop nucleotides, including 6 of the 7 highly conserved loop residues, but leaves the loop structure intact (28). Proteins were serially diluted in running buffer to the concentrations indicated in Figure 2 and injected at 20°C at a flow rate of 50 μl min^{-1} for 1 min. Disruption of any complex that remained bound after a 5 min dissociation was achieved using a 1 min injection of 2 M NaCl at 20 μl min^{-1}. Samples with different concentrations of protein were injected

in random order, and every injection was performed in triplicate within each experiment. All experiments were done three to ten times. In order to subtract any background noise from each dataset, all samples were also run over an unmodified sensor chip surface and random injections of running buffer were performed throughout every experiment ['double referencing' (31)]. In the experiments that were designed to determine the effect of NaCl concentrations, the buffer contained NaCl at 220, 330 or 500 mM. Data were processed using Scrubber and analyzed using CLAMP XP (32) (developed by the Center for Biomolecular Interaction Analysis at the University of Utah, www.cores.utah.edu/interaction) and a simple 1:1 Langmuir interaction model with a correction for mass transport (33). The fitting of each data set yielded rates for association (k_a) and dissociation (k_d), from which the equilibrium dissociation constant was calculated ($K_D = k_d/k_a$). The k_a, k_d and K_D from three or more experiments were used to calculate the mean values of these variables and the SEM. The results for all mutants were compared (with the wild-type protein and to each other) using the Student's *t*-test to determine statistical significance. Equal and unequal variance for the samples was determined using the *F*-test.

Molecular dynamics simulations

To study the U1A/U1hpII complex, a 2 ns simulation was carried out, based on the B and Q chains of the X-ray coordinates of human U1A (amino acids 2–97) complexed with the RNA hairpin 5′-AAUCCAUUGCACUCCGG AUUU-3′ (22) (PDB ID: 1URN). Briefly, we removed the 5′ adenine and two uracil bases and extended the stem with a 5 bp RNA helix, in order to better match the RNA used in the Biacore experiments: 5′-AGCUUAUCCAUUGCACUCCGGAUAAGCU-3′ (Figure 1C). The RNA stem extension was added by superimposing a 9 bp duplex RNA (built with the NUCGEN module in AMBER 6) onto the experimentally determined stem, such that 4 bp of the 9 bp duplex were fitted to 4 bp of the experimental structure. The four fitted base pairs of the ideal duplex were then deleted, leaving the 5 bp extension. Since the protein of the X-ray structure was incomplete, it was necessary to complete the partial sidechains for Lys20 and Lys96. In addition, the X-ray structure contained two mutated residues (His31 and Arg36), which were mutated back to the wild-type residues, Tyr31 and Gln36, respectively. The mutated protein residues and the RNA backbone atoms connecting the X-ray structure to the NUCGEN-built RNA stem extension were relaxed using a 3000-step minimization *in vacuo*, in which all other atoms were restrained. Water molecules present in the X-ray structure were retained for the simulation, except that the removal of 8 of these 157 water molecules was necessary to allow the positioning of the extended RNA stem and the sodium counterions (crystal water molecules closer than 1 Å to the atoms of the extended RNA stem were removed). Using LeaP, sodium ions were added to make the complex electroneutral (22 ions). The simulation was run using the SANDER module of AMBER 6.0 and SHAKE (34) was applied to all hydrogen atoms. Equilibration of the solvent molecules was achieved by first raising the temperature of the system to 298 K during the first 10 000 steps (100 ps) with position-restraint of all protein atoms with a force constant of 20 kcal/(mol Å). The solute atoms remained so constrained for another 40 000 steps, allowing the water to relax around the solute at 298 K. After this equilibration period, all subsequent simulations were run using the interpolated particle mesh Ewald method to determine Lennard-Jones and electrostatic interactions (35). Following the 100 ps solute-restrained period, the restraint on the solute atoms was removed and a 2 ns simulation was performed, the first 100 ps of which was considered to be part of the equilibration of the system. The target pressure was 1 atm, the time constant was 0.002 ps, and the Lennard-Jones cutoff was 8 Å. The simulation system included 27 496 atoms and contained 8333 water molecules in a box of dimensions

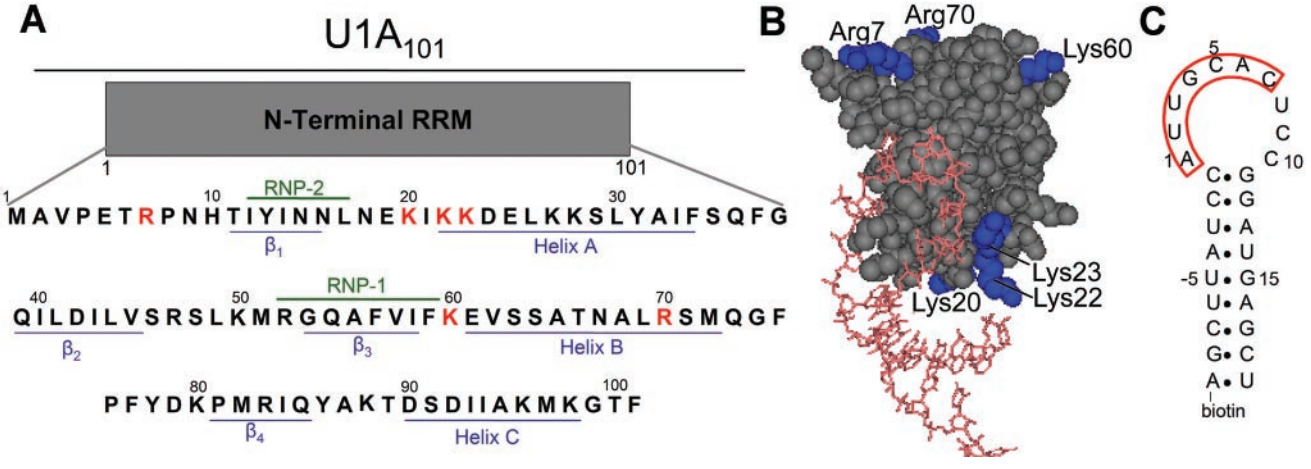

Figure 1. Representation of the protein, protein–RNA complex and RNA target. (**A**) The amino acid sequence of the N-terminal RRM of U1A showing structural features in blue, conserved RNP domains in green, and positively charged amino acids mutated in this study in red. (**B**) Space filling model of the U1A/U1hpII complex as taken from the X-ray crystal structure (22) (pdb ID 1URN). Highlighted in blue are the positively charged residues mutated in this study; the RNA target is indicated in red. For orientation purposes, Lys20 is pointing into the plane away from the viewer, while Lys22 is pointing out of the plane towards the viewer. (**C**) U1hpII RNA used in our kinetic analyses. Nucleotides U-5 to G15 are identical to the wild-type RNA target. The numbering scheme is based on the loop residues numbered 1 through 10, with backward and forward numbering used for the 5′ and 3′ ends of the stem, respectively. The loop residues essential for high affinity U1A binding are seen in a red box; the 5′ A carries the biotin linker.

72.5 × 59.1 × 81.9 Å. The simulation data were analyzed as follows: individual atom interactions between protein and RNA atoms were identified using the analysis algorithm PRORNA (E. J. Chambers, M. J. Law, K. A. Patel, M. Z. Bayramyan and I. S. Haworth, manuscript in preparation). Other analyses were performed using PTRAJ in AMBER 6 and MOLTOOL (I. S. Haworth, unpublished algorithm). Simulation dynamics were visualized using VMD (36).

RESULTS AND DISCUSSION

Choice of mutated residues

We used the co-crystal structure of the N-terminal RRM of U1A complexed with U1hpII (22) to determine which residues would be appropriate to study. As our goal was to dissect the role of electrostatics in the interaction, we selected positively charged residues of which the side chains are not implicated in any hydrogen bonding with the RNA. We focused on two areas of the RRM for study. The first was the region close to the RNA stem, containing Lys20, Lys22 and Lys23 (Figure 1A and B), the former two of which had been shown previously to play a role in association (14). Our goal was to examine the role of individual amino acids in this region of the protein. We hypothesized that they would be required for optimal association. For comparison, we also studied a second region of the RRM that lies far from the RNA in the complex. This region, which is located 'on top' of the polypeptide, has three positively charged residues, Arg7, Lys60 and Arg70, which form a triangle at the crown of the molecule (Figure 1B). We hypothesized that positive charge in this area might play a role in binding, either assisting in the general attraction of the RNA, or in fact interfering with RNA recruitment by attracting the RNA to the wrong side of the molecule. For the current studies we elected not to make mutations to non-polar alanine residues (as in our previous studies), but instead mutated the residues to glutamine, resulting in the replacement of positively charged side chains by uncharged polar side chains while maintaining a similar side chain length.

Charged crown residues have little effect on U1A/U1hpII binding kinetics

We began our investigation by examining the RNA-binding kinetics of proteins in which Arg7, Lys60 and Arg70 had been individually mutated to Gln. A U1hpII RNA surface (Figure 1C) was generated on a Biacore sensor chip, and proteins were injected at different concentrations. Association and dissociation rates were calculated by fitting the data to a simple 1:1 interaction model including a step to account for mass transport (Figure 2) (32). Binding of the Arg7Gln mutant was kinetically similar to that of wild-type U1A. Interestingly, the Lys60Gln and Arg70Gln mutants both associated slightly faster than wild-type U1A (Table 1 and Figure 3) and formed a complex that was slightly (statistically significantly) less stable than wild type. These results suggested that these residues, positioned far from the RNA interface, might play a small negative role in complexation, presumably by attracting the RNA to the wrong side of the protein. To further investigate this, we designed triple mutants, changing the three residues simultaneously to either Gln or Glu (Figure 2). The triple mutants did not bear out a clear role of the crown residues in the interaction with the RNA (Table 1 and Figure 3); mutation of all three residues to Gln caused no significant changes in kinetic behavior compared with wild-type U1A. Mutation to Glu appeared to cause a small, significant decrease in association, and a minor impact on complex stability. In combination, they had a very modest negative effect on the affinity, perhaps through general repulsion of the RNA. Taken together, these results indicate that charged residues on the crown of the RRM have a minor contribution to the overall electrostatic interactions of U1A with U1hpII. This suggests that positively charged amino acids far away from the RNA-binding surface of an RNA-BP do not play a very significant role in RNA binding.

Multiple roles for charges close to the interaction interface

We continued our investigation by mutating residues close to the RNA interface: Lys20, Lys22 and Lys23 were changed individually into Gln. The solvent exposure, proximity to the RNA, and previous mutational analyses of Lys20, Lys22 and Lys23 suggested that these residues would be prime candidates for important electrostatic interactions. A previous investigation of individual Lys22 and Lys23 mutations by another laboratory had indicated that substitutions of these residues result in a loss of RNA-binding affinity (26). Examination of the co-crystal structure shows Lys20 and 22 positioned close to the phosphate backbone of the RNA stem, while Lys23 is located on helix A of the protein close to RNA loop nt 8–10 [Figure 1, (22)]. Loop nt 1–7, which form a rigid network of close range interactions with the protein, are required for specific binding, while loop nt 8–10 are thought to be somewhat mobile (22,37–39). The latter 3 nt are structurally important, but their sequence is irrelevant (28,37,40). Their position near Lys23 suggests that one or more of these nucleotides could interact with this residue (Figure 1B).

The binding kinetics of mutants Lys20Gln, Lys22Gln and Lys23Gln interacting with U1hpII were examined (Figure 2). Each showed a statistically significant ~2- to 3-fold decrease in association rate when compared with wild-type U1A (Table 1 and Figure 3). In addition to this association defect, Lys22Gln also showed a statistically significant 3-fold decrease in complex stability. In contrast, the small decrease in complex stability for Lys23Gln was not statistically different from wild-type U1A. While the impact of the mutations on affinity were modest, these results suggest that all of these positively charged residues in U1A play a role in RNA binding, albeit in different aspects of the interaction. To investigate further, a series of double and triple mutants were constructed and the kinetics of their interaction with U1hpII were examined.

First we simultaneously mutated Lys20 and Lys22 to Arg, Gln and Glu (Lys20Lys22Arg, Lys20Lys22Gln and Lys20Lys22Glu) (Table 1 and Figures 2 and 3). The binding kinetics of the Lys20Lys22Arg mutant were not statistically significantly different from that of wild-type U1A, showing that substitution to a different positively charged residue is well tolerated, and supporting the idea that the role of these residues is related primarily to their charge. In contrast,

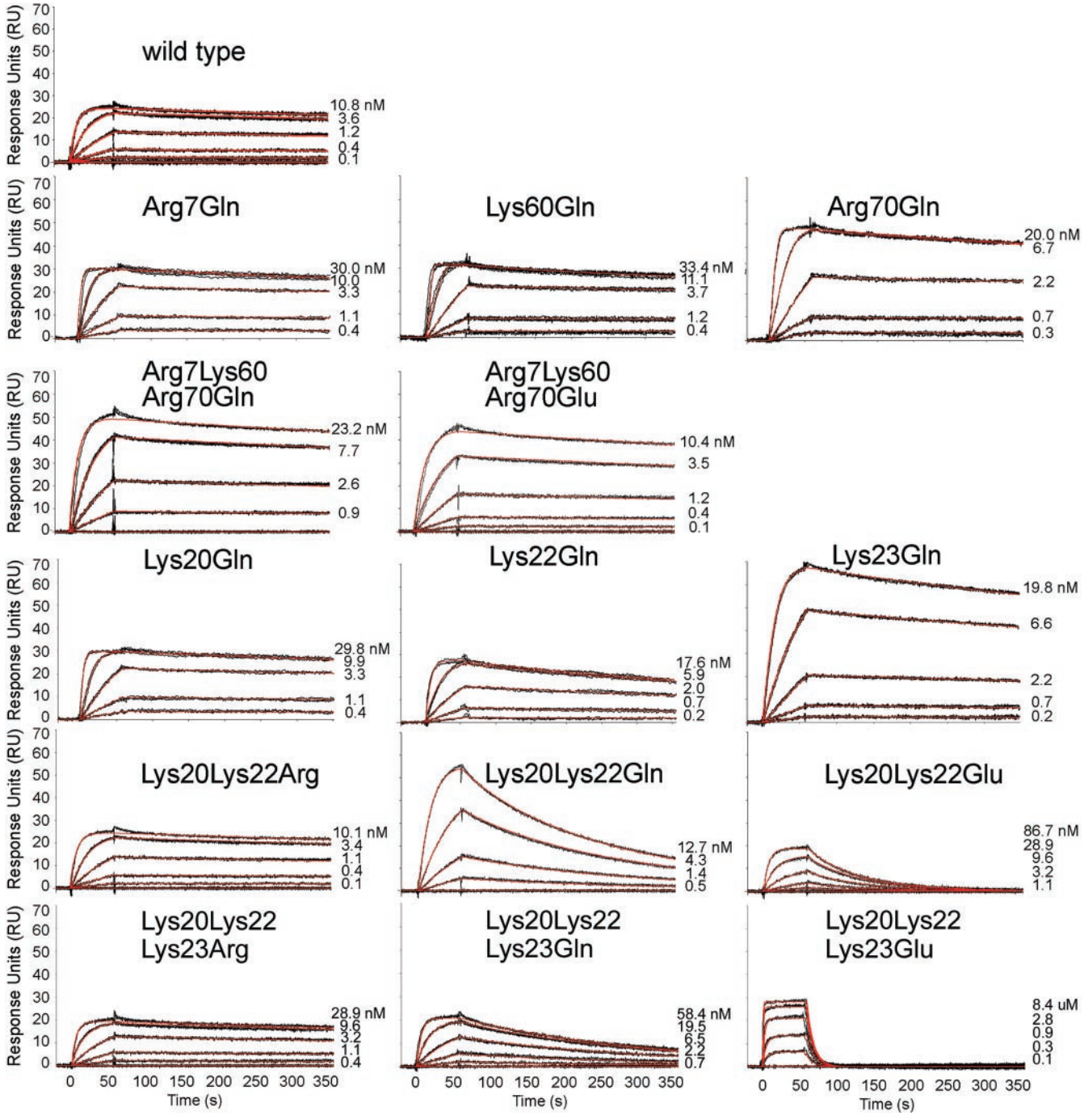

Figure 2. Sensorgrams showing kinetic analyses of wild-type U1A and mutant proteins with U1hpII RNA. Black lines represent triplicate injections which were performed in random order over a U1hpII surface at the indicated concentrations. Association was monitored for 1 min followed by a 5 min dissociation phase. Red lines represent the global fit of datasets using CLAMP (32). Kinetic parameters for the experiments are shown in Table 1.

the Lys20Lys22Gln and Lys20Lys22Glu mutants showed increasing defects in the interaction with RNA. The association rate defect of Lys20Lys22Gln was twice that of the individual Gln mutants (~4-fold loss, $P < 0.001$), showing an additive effect. In contrast, the effect of the double Gln mutation on stability was similar to that of Lys22Gln alone (~3-fold, $P < 0.001$). The relatively stronger effect of a double Lys20Lys22 mutant on association versus dissociation had been noted earlier when these residues had been simultaneously replaced by alanine (14), but those earlier experiments did not distinguish between the roles of the two lysines. Here it becomes clear that the stability defect arises from mutation of Lys22. When the two lysines were replaced by Glu instead of Gln, the loss is association was doubled (~8-fold, $P < 0.001$) and the complex was almost 30-fold less stable than the wild type. Thus, addition of negative charge close to the phosphate backbone not only slows association, but also destabilizes the protein–RNA complex.

Table 1. Kinetic parameters for U1A and mutants interacting with U1hpII[a]

Protein	k_a($M^{-1}s^{-1}$)	Fold decrease[b] k_aWT/$k_a$mut	k_d(s^{-1})	Fold increase[b] $k_d$mut/k_dWT	K_D(M)	Fold increase[b] $K_D$mut/K_DWT
Wild type	$(1.22 \pm 0.08) \times 10^7$		$(4.8 \pm 0.2) \times 10^{-4}$		$(4.0 \pm 0.2) \times 10^{-11}$	
Arg7Gln	$(1.2 \pm 0.2) \times 10^7$	1.0	$(6.1 \pm 0.7) \times 10^{-4}$	1.3	$(5 \pm 1) \times 10^{-11}$	1.3
Lys60Gln	$(2.2 \pm 0.4) \times 10^7$	0.5	***(7.1 ± 0.6) × 10⁻⁴***	1.5	$(3.3 \pm 0.3) \times 10^{-11}$	0.8
Arg70Gln	***(1.93 ± 0.09) × 10⁷***	0.6	***(6.4 ± 0.4) × 10⁻⁴***	1.3	$(3.4 \pm 0.3) \times 10^{-11}$	0.8
Arg7Lys60Arg70Gln	$(1.1 \pm 0.1) \times 10^7$	1.1	$(4.4 \pm 0.1) \times 10^{-4}$	0.9	$(4.3 \pm 0.5) \times 10^{-11}$	1.1
Arg7Lys60Arg70Glu	***(9 ± 1) × 10⁶***	1.4	$(8 \pm 2) \times 10^{-4}$	1.6	***(9 ± 1) × 10⁻¹¹***	2.2
Lys20Gln	***(5 ± 1) × 10⁶***	2.1	$(4.5 \pm 0.1) \times 10^{-4}$	0.9	$(9 \pm 3) \times 10^{-11}$	2.2
Lys22Gln	***(6 ± 1) × 10⁶***	1.9	***(1.5 ± 0.2) × 10⁻³***	3.1	$(3 \pm 1) \times 10^{-10}$	7.2
Lys23Gln	***(4.3 ± 0.9) × 10⁶***	2.8	$(8 \pm 2) \times 10^{-4}$	1.8	***(1.9 ± 0.2) × 10⁻¹⁰***	4.8
Lys20Lys22Arg	$(9 \pm 1) \times 10^6$	1.3	$(4.2 \pm 0.2) \times 10^{-4}$	0.9	$(4.6 \pm 0.5) \times 10^{-11}$	1.2
Lys20Lys22Gln	***(2.8 ± 0.2) × 10⁶***	4.3	***(1.38 ± 0.01) × 10⁻³***	2.9	***(5.0 ± 0.5) × 10⁻¹⁰***	12
Lys20Lys22Glu	***(1.57 ± 0.09) × 10⁶***	7.8	***(1.39 ± 0.09) × 10⁻²***	29	***(8.9 ± 0.3) × 10⁻⁹***	220
Lys20Lys22Lys23Arg	***(5.64 ± 0.07) × 10⁶***	2.2	***(5.8 ± 0.2) × 10⁻⁴***	1.2	***(1.03 ± 0.04) × 10⁻¹⁰***	2.6
Lys20Lys22Lys23Gln	***(3.7 ± 0.4) × 10⁶***	3.4	***(4.2 ± 0.2) × 10⁻³***	8.6	***(1.2 ± 0.4) × 10⁻⁹***	29
Lys20Lys22Lys23Glu	***(2.7 ± 0.2) × 10⁵***	45	***(1.13 ± 0.02) × 10⁻¹***	230	***(4.3 ± 0.3) × 10⁻⁷***	11 000

[a]The K_D was calculated for each independent Biacore experiment from the fitted k_a and k_d ($K_D = k_d/k_a$). The k_a, k_d and K_D from three or more experiments were used to calculate the mean values of these variables and the SEM. Values in bold italics represent statistically significant differences from wild type ($P < 0.05$).
[b]The ratios in the fold change columns have been chosen to most frequently show a positive number: WT/mut for k_a, mut/WT for k_d and K_D. The numbers given are approximations, shown to two significant digits.

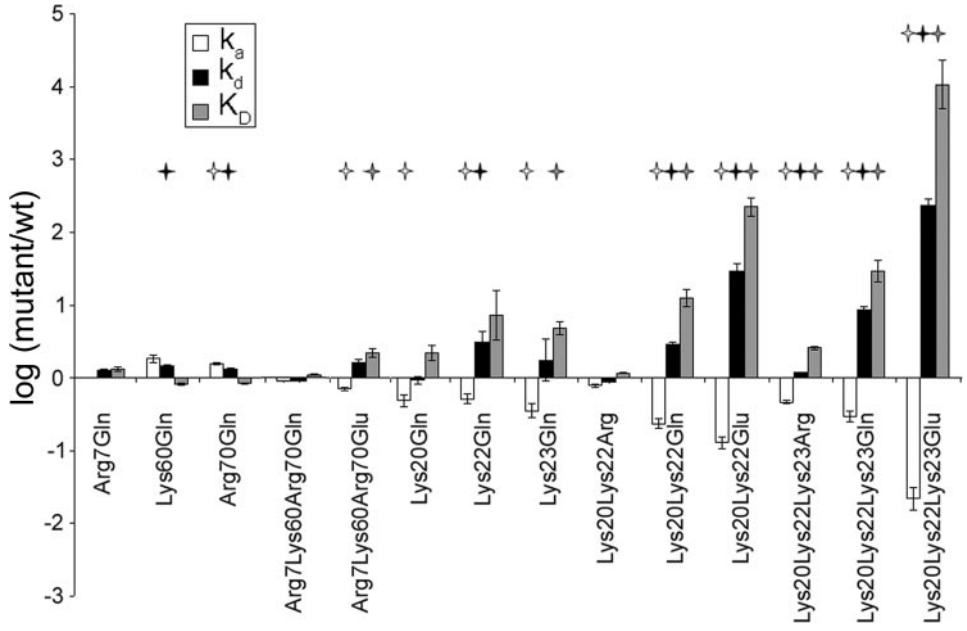

Figure 3. Effects of electrostatic mutations on k_a, k_d and K_D. To visualize the differences between mutants and wild type protein, we plotted the logarithm of wild type/mutant values for k_a (open bars) and mutant/wild-type values for k_d (gray bars) and K_D (closed bars). Error bars indicate the SEM while stars represent values that are statistically significantly different from wild type.

We next added the mutation of Lys23, making triple mutants in which Lys20, Lys22 and Lys23 were simultaneously mutated to Arg, Gln or Glu. Lys20Lys22Lys23Arg showed small but statistically significant differences in association and dissociation rates and affinity compared with wild-type U1A (Table 1 and Figure 3). These differences were, however, not significant when compared with Lys20Lys22Arg. Thus, the cumulative Arg replacement appears to marginally disturb the interaction with RNA. Addition of the Lys23Gln mutation to the double Gln mutant (Lys20Lys22Lys23Gln) did not add to the association defect, but further decreased the stability of the complex. The ~9-fold loss in complex stability of the triple Gln mutant was statistically significantly different from both wild-type and Lys20Lys22Gln proteins (Table 1 and Figure 3). This indicates that in the absence of positive charge at positions 20 and 22, Lys 23 clearly plays a role in maintaining the integrity of the complex. The insertion of negative charge at the Lys23 position (Lys20Lys22Lys23Glu) was very deleterious to RNA binding, resulting in a loss of affinity of four orders of magnitude compared with wild-type U1A. This loss in affinity was due to a deficiency in both association and complex stability; association of protein and RNA occurred 45-fold more slowly than wild-type U1A and 5-fold more slowly than the Lys20Lys22Glu double mutant, while the triple Glu mutant was ~230-fold less stable than wild-type U1A and almost 10-fold less stable than the Lys20Lys22Glu

double mutant (Table 1 and Figure 3). Thus, addition of negative charge at this position not only impacts the formation of the complex, but has a pronounced effect on the ability of the complex to stay together once it has formed. The further destabilization by addition of a Lys23Glu mutation to the double Glu mutant suggests that Lys23 may interact electrostatically with one or more phosphates of the last 3 nt of the RNA loop.

Effects of increasing the NaCl concentration

To further analyze the electrostatic contribution of Lys20, Lys22 and Lys23 to RNA binding, we analyzed the binding kinetics of the wild-type RRM, double mutants of Lys20Lys22, and triple mutants of Lys20Lys22Lys23 to Arg, Gln or Glu at increasing salt concentrations (220, 330 and 500mM NaCl) (Table 2 and Figure 4). The steep salt dependence of U1A binding had already been reported by us and others, and supports the importance of electrostatic interactions in this system (14,21). If the role of the three targeted lysine residues is to allow proper electrostatic interactions, then increasing the NaCl concentration in the buffer would lead to a loss in RNA-binding affinity of wild-type U1A and Arg mutants. The effect of increased salt concentrations on the kinetic behavior of the Gln mutants would be expected to be reduced due to the removal of charge at these positions (12,41). Accordingly, kinetic analysis of the Glu mutants in increased salt would be expected to show the smallest negative effect (the addition of salt might even mitigate the deleterious effect of the inserted Glu residues).

Examination of the association rates of all proteins tested showed that the greatest impact of increasing ionic strength was on wild-type and the double and triple Arg mutant proteins (Table 2 and Figure 4). Compared with the interaction at 150 mM NaCl, in 500 mM NaCl the wild-type protein showed a 28-fold loss in association rate, and the Lys20Lys22Arg mutant exhibited a similar 21-fold loss. A more substantial 77-fold loss in the association rate of Lys20Lys22Lys23Arg was seen, which could be due to small perturbations of protein structure that affect the local interaction of these amino acids with the RNA. When charge was removed from these positions, as is the case with the double and triple Gln mutants, the decrease in association rate was less marked. At 500 mM NaCl, the Lys20Lys22Gln mutant showed a 17-fold decrease in its association rate and the Lys20Lys22Lys23Gln showed a 13-fold loss, compared with the association rates observed at 150 mM NaCl. The mitigation of the salt effect on these mutants suggests that positive charge in these positions is important for complex formation. Further evidence of the importance of these residues was provided by examination of the double and triple Glu mutants. Lys20Lys22Glu showed a 10-fold loss in association rate, and Lys20Lys22Lys23Glu showed no loss in association when comparing 500 with 150 mM; its association rate actually appeared to improve (Table 2). The replacement of positive charges important for complex formation with negative charges would result in repulsion of the RNA from the protein-binding pocket. Increasing the NaCl concentration could mask this repulsion, thereby alleviating the negative effects of the Glu mutations on association.

Table 2. Effect of NaCl on interaction kinetics of U1A and mutants with U1hpII[a]

	[NaCl] (mM)	k_a ($M^{-1}s^{-1}$)	Fold decrease[b]	k_d (s^{-1})	Fold increase[b]	K_D(M)	Fold decrease[b]
Wild type	150	$(1.22 \pm 0.08) \times 10^7$		$(4.8 \pm 0.2) \times 10^{-4}$		$(4.0 \pm 0.2) \times 10^{-11}$	
	220	$(6.2 \pm 0.4) \times 10^6$	2.0	$(4.27 \pm 0.05) \times 10^{-4}$	0.9	$(7.0 \pm 0.5) \times 10^{-11}$	1.8
	330	$(2.33 \pm 0.09) \times 10^6$	5.3	$(5.4 \pm 0.4) \times 10^{-4}$	1.1	$(2.3 \pm 0.1) \times 10^{-10}$	5.8
	500	$(4 \pm 1) \times 10^5$	28	$(1.31 \pm 0.09) \times 10^{-3}$	2.7	$(3.2 \pm 0.4) \times 10^{-9}$	81
Lys20Lys22Arg	150	$(1.0 \pm 0.1) \times 10^7$		$(4.2 \pm 0.2) \times 10^{-4}$		$(4.6 \pm 0.5) \times 10^{-11}$	
	220	$(8.4 \pm 0.6) \times 10^6$	1.1	$(4.67 \pm 0.04) \times 10^{-4}$	1.1	$(5.6 \pm 0.3) \times 10^{-11}$	1.2
	330	$(3.0 \pm 1) \times 10^6$	3.2	$(6.8 \pm 0.2) \times 10^{-4}$	1.6	$(2.3 \pm 0.1) \times 10^{-10}$	4.9
	500	$(4.6 \pm 0.3) \times 10^5$	21	$(1.71 \pm 0.01) \times 10^{-3}$	4.1	$(3.8 \pm 0.3) \times 10^{-9}$	82
Lys20Lys22Gln	150	$(2.8 \pm 0.2) \times 10^6$		$(1.38 \pm 0.07) \times 10^{-3}$		$(5.0 \pm 0.5) \times 10^{-10}$	
	220	$(1.48 \pm 0.05) \times 10^6$	1.9	$(2.21 \pm 0.04) \times 10^{-3}$	1.6	$(1.50 \pm 0.04) \times 10^{-09}$	3.0
	330	$(8 \pm 2) \times 10^5$	3.5	$(4.5 \pm 0.1) \times 10^{-3}$	3.2	$(6 \pm 1) \times 10^{-9}$	12
	500	$(1.66 \pm 0.08) \times 10^5$	17	$(1.10 \pm 0.02) \times 10^{-2}$	8.0	$(6.7 \pm 0.4) \times 10^{-8}$	140
Lys20Lys22Glu	150	$(1.57 \pm 0.096) \times 10^6$		$(1.39 \pm 0.09) \times 10^{-2}$		$(8.9 \pm 0.2) \times 10^{-9}$	
	220	$(9.1 \pm 0.2) \times 10^5$	1.7	$(1.74 \pm 0.03) \times 10^{-2}$	1.3	$(1.93 \pm 0.03) \times 10^{-8}$	2.2
	330	$(4.2 \pm 0.5) \times 10^5$	3.7	$(2.6 \pm 0.1) \times 10^{-2}$	1.9	$(6.5 \pm 0.7) \times 10^{-8}$	7.3
	500	$(1.52 \pm 0.08) \times 10^5$	10	$(4.5 \pm 0.1) \times 10^{-2}$	3.2	$(3.0 \pm 0.2) \times 10^{-7}$	34
Lys20Lys22Lys23Arg	150	$(5.6 \pm 0.8) \times 10^6$		$(5.8 \pm 0.2) \times 10^{-4}$		$(1.03 \pm 0.04) \times 10^{-10}$	
	220	$(2.5 \pm 0.2) \times 10^6$	2.3	$(8.1 \pm 0.4) \times 10^{-4}$	1.4	$(3.3 \pm 0.3) \times 10^{-10}$	3.2
	330	$(5.7 \pm 0.2) \times 10^5$	9.8	$(1.21 \pm 0.03) \times 10^{-3}$	2.1	$(2.1 \pm 0.2) \times 10^{-9}$	21
	500	$(7.3 \pm 0.3) \times 10^4$	77	$(2.91 \pm 0.02) \times 10^{-3}$	5.0	$(4.0 \pm 0.2) \times 10^{-8}$	390
Lys20Lys22Lys23Gln	150	$(3.7 \pm 0.4) \times 10^6$		$(4.2 \pm 0.2) \times 10^{-3}$		$(1.2 \pm 0.1) \times 10^{-9}$	
	220	$(1.1 \pm 0.1) \times 10^6$	3.2	$(5.7 \pm 0.1) \times 10^{-3}$	1.4	$(5.3 \pm 0.7) \times 10^{-9}$	4.5
	330	$(8.1 \pm 0.6) \times 10^5$	4.5	$(1.38 \pm 0.07) \times 10^{-2}$	3.3	$(1.71 \pm 0.04) \times 10^{-8}$	15
	500	$(2.9 \pm 0.2) \times 10^5$	13	$(2.5 \pm 0.2) \times 10^{-2}$	6.1	$(8.7 \pm 0.2) \times 10^{-8}$	74
Lys20Lys22Lys23Glu	150	$(2.7 \pm 0.2) \times 10^5$		$(1.13 \pm 0.02) \times 10^{-1}$		$(4.3 \pm 0.3) \times 10^{-7}$	
	220	$(3.9 \pm 0.7) \times 10^5$	0.7	$(2.2 \pm 0.5) \times 10^{-1}$	1.9	$(5.5 \pm 0.7) \times 10^{-7}$	1.3
	330	$(2.4 \pm 0.3) \times 10^5$	1.1	$(1.32 \pm 0.04) \times 10^{-1}$	1.2	$(5.9 \pm 0.8) \times 10^{-7}$	1.4
	500	$(9 \pm 2) \times 10^5$	0.3	(2.3 ± 0.4)	20	$(4 \pm 1) \times 10^{-6}$	8.3

[a]The K_D was calculated for each independent Biacore experiment from the fitted k_a and k_d ($K_D = k_d/k_a$). The k_a, k_d and K_D from three or more experiments were used to calculate the mean values of these variables and the SEM.
[b]Fold difference compared with the same protein tested in 150 mM NaCl is indicated.

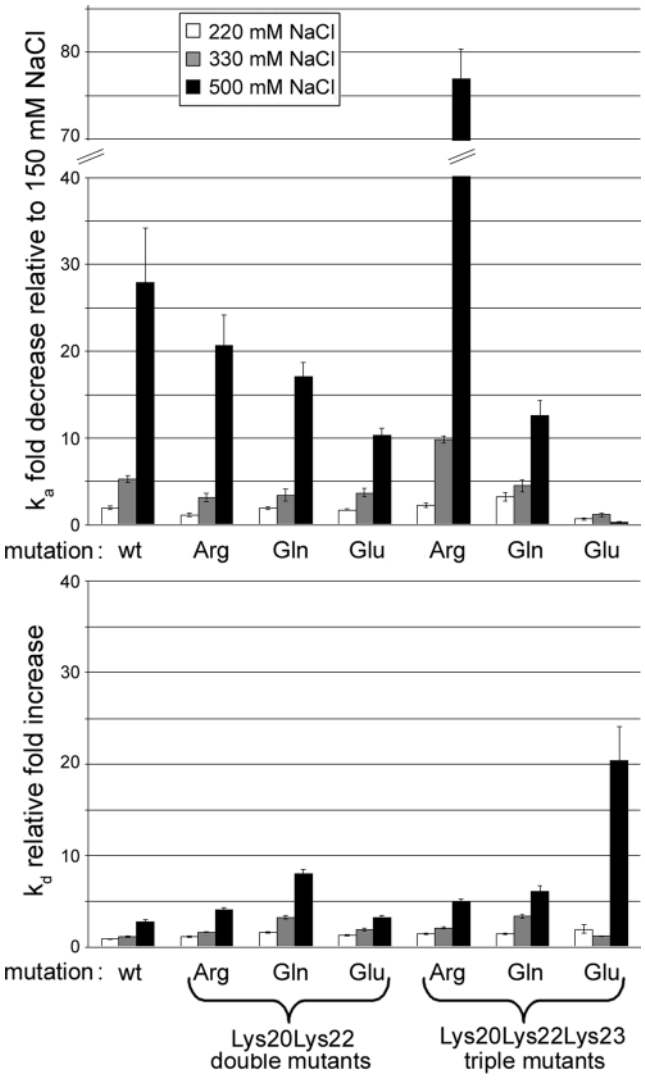

Figure 4. The effect of salt concentration on the behavior of U1A and its mutants. Upper panel: bars represent the loss in association rate for each protein at 220 (open), 330 (gray) and 500 (closed) mM NaCl, compared with 150 mM NaCl. Note that for the triple Glu mutant there is actually a relative gain in the association rate at 220 and 550 mM NaCl (Table 2). Lower panel: bars indicate the increase in dissociation rate for each protein at 220, 330 and 500 mM NaCl, compared with 150 mM NaCl. The SEM is indicated by error bars.

As we had reported previously, complex stability does not seem to be affected as strongly as association by changes in NaCl concentration (14). In fact, a 1 min injection of 2 M NaCl is required to fully remove bound protein and regenerate the RNA surfaces on the Biacore sensor chip. This salt resistance is not unexpected, as the picomolar affinity of the U1A/U1hpII complex results from numerous stacking and hydrogen-bonding interactions, and electrostatics presumably play a minor role. Thus, removal of the electrostatic contribution of the three lysines to complex stability would probably not greatly increase susceptibility to disruption by salt. Indeed, the double and triple Gln mutants showed only a slightly increased salt sensitivity, compared with the wild-type and Arg substitution mutants; at 500 mM NaCl the Gln mutants showed ~8- and ~6-fold losses in complex stability compared with ~3- to ~5-fold losses for the wild-type and Arg mutant proteins (Table 2 and Figure 4, lower panel). In the case of Glu substitutions, the consequences would be difficult to predict; increased salt might mitigate the effect of the Glu residues on complex stability; however, the added negative charge could also make the weakened complex more prone to salt disruption. Interestingly, both effects appear to be evident: the double Glu mutant showed a very modest ~3-fold loss in complex stability in 500 mM NaCl compared with 150 mM salt (Table 2 and Figure 4). The RNA/bound complex of the triple Glu mutant seemed similarly resistant to increased salt concentrations up to 330 mM. However, in 500 mM NaCl the mutant complex was ~20-fold less stable than it was in 150 mM NaCl (Table 2 and Figure 4). It is likely that the threshold NaCl concentration at which the protein–RNA complex is disrupted is lower for the already unstable complex of U1hpII with the triple Glu mutant.

In summary, the salt dependence experiments confirm the important role electrostatics play in bringing RNA and protein together; the ionic shielding of charged residues at higher salt concentrations reduced the mutual attraction of protein and RNA. Conversely, removal of charge at the lysines reduced the negative effect of increased salt concentrations on those mutants because fewer positive residues were present. Complex dissociation appeared less prone to the effect of salt, perhaps because once established, electrostatic interactions may be less liable to be disrupted if they are partially shielded in the complex. This would explain the more pronounced effect of mutations versus increased salt on complex stability; when the Lys residues are mutated to Glu permanent negative charges are built into the protein.

Molecular dynamics simulations reveal different roles for positively charged residues

Our kinetic analyses point to distinct roles of the three lysine residues at positions 20, 22 and 23 in the U1A/U1hpII interaction. Lys20 would appear to be predominantly involved in complex formation, as the Lys20Gln mutant displays no deficiency in complex stability, but association is affected (Table 1 and Figure 3). In contrast, Lys22 seems to be important for both association and stability of the complex, as the Lys22Gln mutant is deficient in both of these parameters. Kinetic measurements of the Lys20Lys22 double mutant supports this idea: the association defects of Lys20Lys22Gln are additive compared with the individual glutamine mutants, but the stability defects are equivalent to that of Lys22Gln alone (Table 1 and Figure 3). The effect of mutating Lys23 is interesting. Although the single Lys23Gln mutant is predominantly deficient in association, the triple mutant data suggest that a mutation in this position in the context of the Lys20Lys22 double mutant does not affect association, but rather stability of the complex (Table 1 and Figure 3). In addition, introduction of negative charge in the glutamic acid mutants causes a dramatic destabilization of the protein–RNA complex. This indicates that neutralization of the negative charge inherent to the RNA target is important. The difference in the roles of Lys20 and Lys22 is intriguing, particularly considering that the position of Lys20 and Lys22 is very similar in the protein–RNA complex; both residues lie close to the RNA stem in the co-crystal structure. In contrast, Lys23 lies in an α-helix close to the RNA loop. In order to gain a better understanding

of the role of these residues in complex stability, we undertook molecular dynamics simulations of the U1A/U1hpII complex.

As a starting point, we used the U1A/U1hpII complex X-ray structure (22). Following initial minimization, the 2 ns simulation showed both Lys20 and 22 interacting with the phosphate backbone of the RNA stem: Lys20 forms a salt bridge to the phosphates at positions C-2 and U-3, while Lys22 is close to the phosphates at positions A-4 and U-5 (Figure 5). Interactions of Lys20 and 22 with the phosphates of stem nucleotides in this region had been noted in a previous 1.2 ns simulation by Tang and Nilsson (20). In our simulation, these interactions appeared to shift at 800–1000 ps into the simulation, when Lys20 formed a closer interaction with the phosphate at U-3 than the one at C-4, and Lys22 'slid' down the stem to form stable interactions with the U-6 and U-5 phosphates (Figure 5). Comparison of the stability of these two interactions over time suggests why mutation of Lys22 to Gln results in a more unstable complex than Lys20 mutation: while both Lys20 and 22 periodically move away from the phosphate backbone, the interaction of Lys22 with the RNA is much more consistent than that of Lys20. Loss of the interaction at position 22 would therefore be expected to compromise complex stability more than loss of the Lys20 interaction. Comparison of these results to five other simulations of wild-type U1A and mutants (mutations distant from the lysines) confirms the role of Lys 20 and 22 (data not shown). In four of them, the interaction of Lys22 with the stem is more consistent than that of Lys20. Furthermore, the simulation of Tang and Nilsson (20), performed on U1A RRM1 interacting with a U1hpII with a slightly shorter stem than we used, showed the same trends in the original simulation. Extension of this simulation to 2 ns showed Lys22 interacting with the stem ~65% of the time, and Lys20 ~40% of the time (data not shown). For Lys22 this is probably an underestimate because in our simulations, it tends to interact with the phosphate of the nucleotide at position −5 and −6 in the stem (Figure 1C), which are absent in the RNA Tang and Nilsson used (20). The importance of the stem contacts for U1A binding is supported by studies of an almost stem-less U1hpII, in which a 2 bp stem is held together by a disulfide crosslink (41). Such an RNA is bound with a >100-fold weaker affinity.

Our 2 ns simulation also indicated that Lys23 is involved in charge-based interactions with the RNA backbone; it interacts with the C10 phosphate in the U1hpII loop (Figure 5). This interaction, which had also been observed by Tang and Nilsson (20) appears to be quite stable, and mutation of Lys23 to Gln would abolish this. Because Lys23 interacts with the phosphate backbone, the bases, which do not make any specific contacts, would remain very mobile compared with loop nt 1–7, as seen in simulations of the complex [data not shown, (20,39)]. The mobility of this region is further underscored by the fact that the Lys23-C10 interaction is seen in only two of the five other wild-type or mutant U1A simulations we evaluated. It has been reported that nt 8–10 of the RNA loop can be replaced by a polyethylene glycol linker without affecting the binding affinity (40). This would suggest that interaction with the phosphate oxygens at this position of the RNA are not crucial, which is in agreement with the modest effect of the single Lys23Gln mutation on complex stability. However, in the context of loss of other stabilizing interactions (such as a Lys22 mutation), the contacts between the loop phosphates and Lys23 may play a more important role. The strong deleterious effect of the triple Glu mutations, which probably cause repulsion of the RNA stem as well as loop, support this idea.

Implications for the binding of RRM-containing proteins

This study has provided evidence for multiple roles of positively charged non hydrogen-bonding amino acids in protein–RNA interactions. Utilizing the well-characterized interaction of U1A with U1hpII as a model system, we have examined the impact of positive charge located either far away from the RNA-binding pocket (on the 'crown' of the protein) or close to the RNA-binding surface. The residues we examined are fully conserved in U1A from a wide variety of vertebrates and all but Arg7 are conserved in *Drosophila* U1A. Mutational analysis of residues Arg7, Lys60 and Arg70 did not reveal a clear role for these amino acids in the interaction with U1hpII. It has been reported that charged residues can contribute significantly to RNA binding even at distances up to 11 Å (12); however, the 'crown' residues are further away,

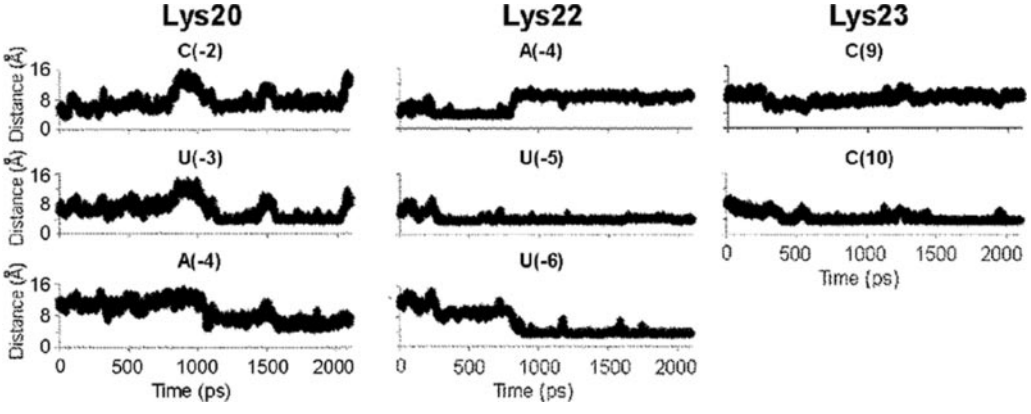

Figure 5. Interactions of Lys20, Lys22 and Lys23 with RNA phosphates during a 2 ns molecular dynamics simulation of the U1A/U1hpII complex. Each plot shows the distance between the N-zeta group of the indicated amino acid and the phosphorous atom of the indicated base over time. Note that the Lys22 interactions are much more consistent than those of Lys20, and that Lys23 interacts with the C10 phosphate but not with that of C9.

and located on a surface location incompatible with the position of bound RNA in the final complex. In fact, positive charge away from the binding site might be expected to be deleterious due to attraction of the RNA to the wrong side of the molecule. However, we found no evidence for this, as mutation of these residues to remove their positive charge was not beneficial to RNA binding. This may be because in the wild-type protein their positive charge is compensated somewhat by acidic residues in the region, such as Glu5, Glu61 and Asp90. However, we also find such residues near Lys20, Lys22 and Lys23, and this does not preclude participation in RNA binding. It should be noted that our studies with the N-terminal U1A RRM and U1hpII do not exclude the possibility that Arg7, Lys60 and Arg70 may play an RNA-binding role in the context of full length U1A interacting with the complete U1 snRNA.

Mutation of residues near the RNA-binding pocket, Lys20, Lys22 and Lys23, shows that these three amino acids are important for the interaction of U1A with U1hpII, and that they play different roles when interacting with the RNA. Our salt-based kinetic analysis reveals the importance of positive charges close to the RNA phosphate backbone. In both wild type and Arg mutants, we see a large salt dependence of association. Removal of charge at these locations (Lys20Lys22Gln and Lys20Lys22Lys23Gln) results in a reduction of the salt dependence, indicating that positive charge in this region is important for the attraction of RNA to the binding pocket. Accordingly, addition of negative charge is deleterious to proper binding. Complex stability seems less drastically impacted by increasing ionic strength. This is probably due to the fact that the stability of the protein–RNA complex is mainly based on hydrogen-bonding and stacking interactions, a large number of which hold protein and RNA together. Basic amino acids playing roles similar to Lys20, Lys22 and Lys23 have been identified on the periphery of the RNA-binding pocket in ribosomal protein L11 and the phage lambda N protein (12,13), although their function in the kinetics of binding remain to be determined.

The different roles of Lys20 and Lys22 are interesting, since these amino acids are located in similar positions and form similar interactions with the RNA stem in the protein–RNA complex. The molecular dynamics simulations revealed that the residence time of each amino acid close to the phosphate backbone differs, and this may explain their unequal contributions to complex stability. Where do the lysine side chains move to when they are away from the phosphate backbone? Preliminary investigation of the motion of the lysines suggests that these residues may interact with negatively charged amino acids elsewhere within the U1A protein. If this is true, then one could envision a scenario in which the negatively charged phosphate backbone competes with negatively charged amino acids in the protein for interactions with Lys20 and Lys22. These competing residues need not lie close to the RNA-binding surface, but must be within reach of the lysines. Removal of such competing negative charges in the protein could allow a more stable protein–RNA interaction. This raises the interesting possibility that the ability of proteins to dissociate from RNA could be modulated by competing local charges, and thus that the affinity of proteins for their targets could be influenced by residues that do not directly contact the RNA. We are currently investigating this possibility through mutational analysis, using the U1A model system.

Although a number of studies have focused in detail on the role of electrostatics in RNA–protein interaction (e.g. 6–13), much about the function of electrostatic interactions in protein–RNA complexes remains to be investigated. Our analysis of the U1A/U1hpII complex provides an example of the role of electrostatics in an RRM/RNA interaction. The examination of structures of other RRM proteins bound to RNA suggests that electrostatic interactions play comparable roles in these complexes. Two examples are the solution structure of nucleolin complexed with snRNE RNA (42), and the co-crystal structures of the neuronal protein HuD, complexed with its AU-rich RNA targets (43). Nucleolin contains four RRMs, but the N-terminal two RRMs bind to a stem–loop RNA target with nanomolar affinity. Similar to the charge-based interactions observed in the U1A/U1hpII complex, positively charged amino acids Lys55 and Lys95 appear to interact with the phosphate backbone of the RNA loop and stem, respectively. HuD contains three RRMs, but the N-terminal two RRMs provide the main RNA-binding ability (44). The two RRMs lie side by side, and form a large RNA-binding platform across which the linear, unstructured AU-rich RNA is draped. Similar arrangements are seen in other two-RRM complexes with linear RNA targets (45,46). In the HuD co-crystals, Lys69 and Lys108, and Arg 155, 166 and 172 contact the phosphate backbone, while Lys74 and Arg123 lie in positions that could also be relevant. It would be of considerable interest to determine whether such residues fall into different functional categories like they do in U1A, and whether this is related to the nature of the adjacent amino acids in the local environment. Such knowledge would be useful, not only to gain a better understanding of the mechanisms controlling protein–RNA interaction, but also for the development of designed targeted nucleic acid-binding proteins that might be used to modulate gene expression in a research or clinical setting.

ACKNOWLEDGEMENTS

We gratefully acknowledge helpful comments and criticisms from Laird-Offringa lab members and our USC colleagues, and thank Dr Ralf Langen for suggesting a study of positively charged amino acids distant from the RNA-binding surface. This material is based on work supported by the National Science Foundation under Grant no. MCB-0131782 (to I.A.L.-O) Funding to pay the Open Access publication charges for this article was provided by the National Science Foundation, Grant No. MCB-0131782.

Conflict of interest statement. None declared.

REFERENCES

1. Maris,C., Dominguez,C. and Allain,F.H. (2005) The RNA recognition motif, a plastic RNA-binding platform to regulate post-transcriptional gene expression. *FEBS J.*, **272**, 2118–2131.
2. Varani,G. and Nagai,K. (1998) RNA recognition by RNP proteins during RNA processing. *Ann. Rev. Biophys. Biomol. Struct.*, **27**, 407–445.
3. Burd,C.G. and Dreyfuss,G. (1994) Conserved structures and diversity of functions of RNA-binding proteins. *Science*, **265**, 615–621.
4. Birney,E., Kumar,S. and Krainer,A.R. (1993) Analysis of the RNA-recognition motif and RS and RGG domains: conservation in metazoan pre-mRNA splicing factors. *Nucleic Acids Res.*, **21**, 5803–5816.

5. Nagai,K., Oubridge,C., Ito,N., Avis,J. and Evans,P. (1995) The RNP domain: a sequence-specific RNA-binding domain involved in processing and transport of RNA. *Trends Biochem Sci*., **20**, 235–240.
6. Chin,K., Sharp,K.A., Honig,B. and Pyle,A.M. (1999) Calculating the electrostatic properties of RNA provides new insights into molecular interactions and function. *Nature Struct. Biol*., **6**, 1055–1061.
7. Misra,V.K. and Draper,D.E. (2000) Mg(2+) binding to tRNA revisited: the nonlinear Poisson–Boltzmann model. *J. Mol. Biol*., **299**, 813–825.
8. Tworowski,D., Feldman,A.V. and Safro,M.G. (2005) Electrostatic potential of aminoacyl-tRNA synthetase navigates tRNA on its pathway to the binding site. *J. Mol. Biol*., **350**, 866–882.
9. Tworowski,D. and Safro,M. (2003) The long-range electrostatic interactions control tRNA–aminoacyl–tRNA synthetase complex formation. *Protein Sci*., **12**, 1247–1251.
10. Trylska,J., Konecny,R., Tama,F., Brooks,C.L.III and McCammon,J.A. (2004) Ribosome motions modulate electrostatic properties. *Biopolymers*, **74**, 423–431.
11. Zuberek,J., Jemielity,J., Jablonowska,A., Stepinski,J., Dadlez,M., Stolarski,R. and Darzynkiewicz,E. (2004) Influence of electric charge variation at residues 209 and 159 on the interaction of eIF4E with the mRNA 5′ terminus. *Biochemistry*, **43**, 5370–5379.
12. GuhaThakurta,D. and Draper,D.E. (2000) Contributions of basic residues to ribosomal protein L11 recognition of RNA. *J. Mol. Biol*., **295**, 569–580.
13. Garcia-Garcia,C. and Draper,D.E. (2003) Electrostatic interactions in a peptide–RNA complex. *J. Mol. Biol*., **331**, 75–88.
14. Katsamba,P.S., Myszka,D.G. and Laird-Offringa,I.A. (2001) Two functionally distinct steps mediate high affinity binding of U1A protein to U1 hairpin II RNA. *J. Biol. Chem*., **276**, 21476–21481.
15. Lander,E.S., Linton,L.M., Birren,B., Nusbaum,C., Zody,M.C., Baldwin,J., Devon,K., Dewar,K., Doyle,M., FitzHugh,W. *et al*. (2001) Initial sequencing and analysis of the human genome. *Nature*, **409**, 860–921.
16. Rubin,G.M., Yandell,M.D., Wortman,J.R., Gabor Miklos,G.L., Nelson,C.R., Hariharan,I.K., Fortini,M.E., Li,P.W., Apweiler,R. *et al*. (2000) Comparative genomics of the eukaryotes. *Science*, **287**, 2204–2215.
17. Lu,J. and Hall,K.B. (1995) An RBD that does not bind RNA: NMR secondary structure determination and biochemical properties of the C-terminal RNA binding domain from the human U1A protein. *J. Mol. Biol*., **247**, 739–752.
18. Scherly,D., Boelens,W., van Venrooij,W.J., Dathan,N.A., Hamm,J. and Mattaj,I.W. (1989) Identification of the RNA binding segment of human U1 A protein and definition of its binding site on U1 snRNA. *EMBO J*., **8**, 4163–4170.
19. Lutz-Freyermuth,C., Query,C.C. and Keene,J.D. (1990) Quantitative determination that one of two potential RNA-binding domains of the A protein component of the U1 small nuclear ribonucleoprotein complex binds with high affinity to stem–loop II of U1 RNA. *Proc. Natl Acad. Sci. USA*, **87**, 6393–6397.
20. Tang,Y. and Nilsson,L. (1999) Molecular Dynamics simulations of the complex between human U1A protein and hairpin II of U1 small nuclear RNA and of free RNA in solution. *Biophys. J*., **77**, 1284–1305.
21. Hall,K.B. and Stump,W.T. (1992) Interaction of N-terminal domain of U1A protein with an RNA stem/loop. *Nucleic Acids Res*., **20**, 4283–4290.
22. Oubridge,C., Ito,N., Evans,P.R., Teo,C.H. and Nagai,K. (1994) Crystal structure at 1.92 A resolution of the RNA-binding domain of the U1A spliceosomal protein complexed with an RNA hairpin. *Nature*, **372**, 432–438.
23. Hermann,T. and Westhof,E. (1999) Simulations of the dynamics at an RNA-protein interface. *Nature Struct. Biol*., **6**, 540–544.
24. Varani,L., Gunderson,S.I., Mattaj,I.W., Kay,L.E., Neuhaus,D. and Varani,G. (2000) The NMR structure of the 38 kDa U1A protein–PIE RNA complex reveals the basis for cooperativity in regulation of polyadenylation by human U1A protein. *Nature Struct. Biol*., **7**, 329–335.
25. Avis,J.M., Allain,F.H., Howe,P.W., Varani,G., Nagai,K. and Neuhaus,D. (1996) Solution structure of the N-terminal RNP domain of U1A protein: the role of C-terminal residues in structure stability and RNA binding. *J. Mol. Biol*., **257**, 398–411.
26. Nagai,K., Oubridge,C., Jessen,T.H., Li,J. and Evans,P.R. (1990) Crystal structure of the RNA-binding domain of the U1 small nuclear ribonucleoprotein A. *Nature*, **348**, 515–520.
27. Jessen,T.H., Oubridge,C., Teo,C.H., Pritchard,C. and Nagai,K. (1991) Identification of molecular contacts between the U1 A small nuclear ribonucleoprotein and U1 RNA. *EMBO J*., **10**, 3447–3456.
28. Katsamba,P.S., Bayramyan,M., Haworth,I.S., Myszka,D.G. and Laird-Offringa,I.A. (2002) Complex role of the beta2-beta3 loop in the interaction of U1A with U1 hairpin II RNA. *J. Biol. Chem*., **277**, 33267–33274.
29. Katsamba,P.S., Park,S. and Laird-Offringa,I.A. (2002) Kinetic studies of RNA–protein interactions using surface plasmon resonance. *Methods*, **26**, 95–104.
30. Law,M.J., Katsamba,P.S., Chambers,E.J., Haworth,I.S. and Laird-Offringa,I.A. (2005) Kinetic analysis of the role of the tyrosine 13, phenylalanine 56, and glutamine 54 network in the U1A/U1 hairpin II interaction. *Nucleic Acids Res*., **33**, 2917–2928.
31. Myszka,D.G. (1999) Improving biosensor analysis. *J. Mol. Recog*., **12**, 1–6.
32. Myszka,D.G. and Morton,T.A. (1998) CLAMP: a biosensor kinetic data analysis program. *Trends Biochem. Sci*., **23**, 149–150.
33. Myszka,D.G., Jonsen,M.D. and Graves,B.J. (1998) Equilibrium analysis of high affinity interactions using BIACORE. *Anal. Biochem*., **265**, 326–330.
34. Ryckaert,J.P., Cicciotti,G. and Berendsen,H.J.C. (1977) Numerical integration of the cartesian equations of motion of a system with constraints: molecular dynamics of *n*-alkanes. *J. Comp. Phys*., **23**, 327–341.
35. Darden,T.A., York,D. and Pedersen,L. (1993) Particle mesh Ewald: an Nlog(N) method for Ewald sums in large systems. *J. Chem. Phys*., **98**, 10089–10092.
36. Humphrey,W., Dalke,A. and Schulten,K. (1996) VMD: visual molecular dynamics. *J. Mol. Graph*., **14**, 33–38.
37. Tsai,D.E., Harper,D.S. and Keene,J.D. (1991) U1-snRNP-A protein selects a ten nucleotide consensus sequence from a degenerate RNA pool presented in various structural contexts. *Nucleic Acids Res*., **19**, 4931–4936.
38. Hall,K.B. (1994) Interaction of RNA hairpins with the human U1A N-terminal RNA binding domain. *Biochemistry*, **33**, 10076–10088.
39. Showalter,S.A. and Hall,K.B. (2005) Correlated motions in the U1 snRNA stem/loop 2:U1A RBD1 complex. *Biophys J*., **89**, 2046–2058.
40. Williams,D.J. and Hall,K.B. (1996) RNA hairpins with non-nucleotide spacers bind efficiently to the human U1A protein. *J. Mol. Biol*., **257**, 265–275.
41. Luchansky,S.J., Nolan,S.J. and Baranger,A.M. (2000) Contribution of RNA conformation to the stability of a high-affinity RNA–protein complex. *J. Am. Chem. Soc*., **122**, 7130–7131.
42. Allain,F.H.-T. (2000) Solution structure of the two N-terminal RNA-binding domains of nucleolin and NMR study of the interaction with its RNA target. *J. Mol. Biol*., **303**, 227–241.
43. Wang,X. and Tanaka Hall,T.M. (2001) Structural basis for recognition of AU-rich element RNA by the HuD protein. *Nature Struct. Biol*., **8**, 141–145.
44. Park-Lee,S., Kim,S. and Laird-Offringa,I.A. (2003) Characterization of the interaction between neuronal RNA-binding protein HuD and AU-rich RNA. *J. Biol. Chem*., **278**, 39801–39808.
45. Handa,N., Nureki,O., Kurimoto,K., Kim,I., Sakamoto,H., Shimura,Y., Muto,Y. and Yokoyama,S. (1999) Structural basis for recognition of the tra mRNA precursor by the sex-lethal protein. *Nature*, **398**, 579–585.
46. Deo,R.C., Bonanno,J.B., Sonenberg,N. and Burley,S.K. (1999) Recognition of polyadenylate RNA by the poly(A)-binding protein. *Cell*, **98**, 835–845.